LAWRENCE
LIVERMORE
NATIONAL
LABORATORY

LLNL-JRNL-405448

Calculation of Radiative Corrections to Hyperfine Splitting in p3/2 States

J. Sapirstein, K. T. Cheng

July 17, 2008

Physical Review A

Disclaimer

This document was prepared as an account of work sponsored by an agency of the United States government. Neither the United States government nor Lawrence Livermore National Security, LLC, nor any of their employees makes any warranty, expressed or implied, or assumes any legal liability or responsibility for the accuracy, completeness, or usefulness of any information, apparatus, product, or process disclosed, or represents that its use would not infringe privately owned rights. Reference herein to any specific commercial product, process, or service by trade name, trademark, manufacturer, or otherwise does not necessarily constitute or imply its endorsement, recommendation, or favoring by the United States government or Lawrence Livermore National Security, LLC. The views and opinions of authors expressed herein do not necessarily state or reflect those of the United States government or Lawrence Livermore National Security, LLC, and shall not be used for advertising or product endorsement purposes.

Calculation of Radiative Corrections to Hyperfine Splitting in $p_{3/2}$ States

J. Sapirstein*

Department of Physics, University of Notre Dame, Notre Dame, IN 46556

K. T. Cheng (鄭國錚)†

Lawrence Livermore National Laboratory, Livermore, CA 94550

(Dated: July 15, 2008)

Abstract

A recent calculation of the one-loop radiative correction to hyperfine splitting (hfs) of $p_{1/2}$ states that includes binding corrections to all orders is extended to $p_{3/2}$ states. Nuclear structure plays an essentially negligible role for such states, which is highly advantageous, as difficulties in controlling the Bohr-Weisskopf effect complicate the isolation of QED contributions for both $s_{1/2}$ and $p_{1/2}$ states. Three cases are studied. We first treat the hydrogen isoelectronic sequence, which is completely nonperturbative in $Z\alpha$ for high Z. Secondly the lowest lying $p_{3/2}$ states of the neutral alkalis are treated, and finally lithiumlike bismuth, where extensive theoretical and experimental studies of the hfs of $2s$ and $2p_{1/2}$ states have been made, is addressed.

PACS numbers: 12.20.Ds, 31.30.Gs, 31.30.jn

*jsapirst@nd.edu

†ktcheng@llnl.gov

I. INTRODUCTION

The Schwinger correction to the electron magnetic moment, $\alpha/2\pi$, while studied with the greatest precision for electrons bound only in a magnetic field [1], was first detected in atomic physics. Although the first accurate determination involved measurements of g-factors in alkalis [2], an earlier indication of the anomaly came from a study of hyperfine splitting (hfs) in the ground state of hydrogen and deuterium [3]. The Fermi formula predicted results distinctly smaller than those measured, and this can be accounted for by modifying the electron magnetic moment by the multiplicative factor $1 + a_e$, where the leading term of the electron anomalous magnetic moment a_e is the Schwinger correction $\alpha/2\pi$ [4]. When dealing with p states the leading term changes to $\alpha/4\pi$ for $p_{1/2}$ states, and $-\alpha/8\pi$ for $p_{3/2}$ states [5]. We have studied the former case in Ref. [6], and the purpose of the present paper is to extend our calculations to the latter case.

The dependence of hfs on the distribution of nuclear magnetism, called the Bohr-Weisskopf (BW) effect [7], substantially affects both s- and $p_{1/2}$-state hfs for highly charged ions, where in the latter case the fact that the lower component of the Dirac wave function behaves as an s state leads to a high overlap of the wave function with the nucleus. There is also a significant BW contribution for heavy neutral alkali metal atoms. However, as the lower component of a $p_{3/2}$ electron behaves as a d state, study of hyperfine splitting in this case is almost completely free of this source of uncertainty. To study this interesting case, most of the theoretical techniques that have been developed to treat s [8–10] and $p_{1/2}$ states [6] can be carried over, with only one part of the calculation needing a new treatment, which will be given in the theory section below. The numerical part of the calculation is, however, considerably more challenging for $p_{3/2}$ states.

As with our previous work on $p_{1/2}$ states, we apply the method to three cases. The first is the isoelectronic sequence of hydrogen. At low nuclear charge Z our results clearly converge to the lowest order result $-\alpha/8\pi$. As is the case with s and $p_{1/2}$ states high values of Z behave in a nonperturbative fashion, and only calculations that treat the electron propagator in an exact manner, as is done here, are valid.

The second application is to neutral alkalis. While these calculations are numerically more difficult than those along the hydrogen isoelectronic sequence, less accuracy is required, as many body uncertainties, with the exception of lithium, are typically much larger than this

radiative correction, so that a relatively straightforward treatment of the latter suffices. We will show that the low Z case has a correction close to $-\alpha/8\pi$, but that cesium and francium change from this result substantially.

We finally treat the case of lithiumlike bismuth. There has been considerable theoretical and experimental work done on the $2s$ and $2p_{1/2}$ hyperfine splittings in this ion, as well as the ground state of hydrogenic bismuth. The large and nonperturbative quantum electrodynamic (QED) effect on hfs for the $1s$ and $2s$ states has unfortunately been obscured by uncertainties in the Bohr-Weisskopf effect. An interesting approach introduced by Shabaev *et al.* [11] has been to form a combination of the hydrogenlike $1s$ and lithiumlike $2s$ measurements that is free of these uncertainties, which we have recently discussed in Ref. [12]. However, while not yet measured, we note that the $2p_{3/2}$ hfs in lithiumlike bismuth as calculated here is by itself essentially free of nuclear uncertainty.

Before we proceed, we should also note that unlike s and $p_{1/2}$ states, there are electric quadrupole (E2) contributions to the hyperfine energies of $p_{3/2}$ states for isotopes with $I \geq 1$. We shall restrict our discussions to the magnetic dipole (M1) hyperfine interactions in this paper.

II. *S*-MATRIX CALCULATION OF HYPERFINE SPLITTING

QED can be applied to the calculation of the spectra of atoms and ions in a systematic fashion through the use of Furry representation [13] or modifications of that representation that incorporate screening [14]. These representations involve the breakup of the full QED Hamiltonian into a lowest order Hamiltonian,

$$H_0 = \int d^3x\, \psi^\dagger(x)\Big[\vec{\alpha}\cdot\vec{p} + \beta m - \frac{Z_{nuc}(r)\alpha}{r} + \tilde{U}(r)\Big]\psi(x) \tag{1}$$

and an interaction Hamiltonian

$$\begin{aligned} H_I \;=\; & -e\int d^3x\, \psi^\dagger(x)\vec{\alpha}\cdot\vec{A}(x)\psi(x) \\ & + \frac{\alpha}{2}\int \frac{d^3x d^3y}{|\vec{x}-\vec{y}|}\,\psi^\dagger(x)\psi(x)\psi^\dagger(y)\psi(y) \\ & - \int d^3x\, \psi^\dagger(x)\tilde{U}(r)\psi(x), \end{aligned} \tag{2}$$

where $r = |\,\vec{x}|$. The case $Z_{nuc}(r) = \tilde{U}(r) = 0$ corresponds to the usual interaction representation of QED and $\tilde{U}(r) = 0$ to Furry representation. When we treat the neutral

alkalis and lithiumlike bismuth we will use a nonvanishing counter potential $\tilde{U}(r)$ such that $U(r) = -Z_{nuc}(r)\alpha/r + \tilde{U}(r)$ corresponds to the same Kohn-Sham potential used in our previous work [6]. If the energy eigenvalue of the Dirac equation in this external potential for a state m is ϵ_m, the lowest order energy will be $\epsilon_{2p_{3/2}}$ for a hydrogenic ion, $2\epsilon_{1s} + \epsilon_{2p_{3/2}}$ for a lithiumlike atom or ions, and $\sum_a (2j_a + 1)\epsilon_a + \epsilon_{np_{3/2}}$ for a general alkali, where the sum over a runs over a noble gas core. Corrections to this lowest order energy are determined through the equation

$$\Delta E = \frac{i\epsilon}{2} \frac{\partial}{\partial \lambda} \langle S_{\epsilon,\lambda} \rangle \tag{3}$$

in the limit $\epsilon \to 0$ and $\lambda \to 1$, and where the S-matrix is defined through

$$S_{\epsilon,\lambda} = T \left[e^{-i\lambda \int dt H_I(t) e^{-\epsilon|t|}} \right]. \tag{4}$$

The S-matrix has a standard representation in terms of Feynman diagrams. Here we are interested in the hyperfine splitting caused by the extra interaction

$$\delta H_I = -e \int d^3x \, \psi^\dagger(\vec{x}, t) \vec{\alpha} \cdot \vec{A}_{\rm ext}(\vec{x}) \psi(\vec{x}, t) \tag{5}$$

where

$$\vec{A}_{\rm ext}(\vec{x}) = \frac{\vec{\mu} \times \vec{r}}{4\pi r^3}, \tag{6}$$

and $\vec{\mu}$ is the magnetic moment of the nucleus. For $p_{3/2}$ states there is no need to modify this form to account for the Bohr-Weisskopf effect, as it enters at a level well under the QED contributions we are interested in here.

Taking δH_I together with two interaction Hamiltonians gives the self-energy and vacuum polarization diagrams shown in Fig. 1 and correlation diagrams shown in Fig. 2. The former radiative diagrams have ultraviolet divergences, which we treat by adding and subtracting diagrams of the same form but with the full electron propagator S_F replaced by the free propagator S_0. For example, in the vertex diagram of Fig. 1b we write the electron line, in a schematic form, as

$$\begin{aligned} S_F(\vec{x}, \vec{y}; E) V(y) S_F(\vec{y}, \vec{z}; E) \; &= \; S_0(\vec{x}, \vec{y}; E) V(y) S_0(\vec{y}, \vec{z}; E) \\ &+ [S_F(\vec{x}, \vec{y}; E) V(y) S_F(\vec{y}, \vec{z}; E) - S_0(\vec{x}, \vec{y}; E) V(y) S_0(\vec{y}, \vec{z}; E)]. \end{aligned} \tag{7}$$

The ultraviolet divergence comes entirely from the first term in the right-hand-side, which is most conveniently evaluated in momentum space. The remaining ultraviolet finite term

is evaluated in coordinate space using partial wave expansions. We use dimensional regularization, in which the dimension of space time is taken to be $n = 4 - \epsilon$, to regularize the ultraviolet divergent term, which is given by

$$\begin{aligned}\nu_{\rm SE}(A) \;=\; & -4\pi i\alpha \int d^3x d^3y d^3z \int \frac{d^nk}{(2\pi)^n}\,\frac{e^{i\vec{k}\cdot(\vec{x}-\vec{z})}}{k^2+i\delta} \\ & \bar{\psi}_v(\vec{x})\gamma_\mu S_0(\vec{x},\vec{y};\epsilon_v-k_0)V(\vec{y})S_0(\vec{y},\vec{z};\epsilon_v-k_0)\gamma^\mu\psi_v(\vec{z}),\end{aligned} \tag{8}$$

with $V(\vec{y}) = -e\vec{\gamma}\cdot\vec{A}(\vec{y})$. Ultraviolet divergences appear as factors of $1/\epsilon$, and after they are canceled by renormalization the limit $\epsilon \to 0$ is taken. The Fourier transformed version of Eq. (8) is

$$\nu_{\rm SE}(A) = -4\pi i\alpha \int d^3p_2\, d^3p_1 \int \frac{d^nk}{(2\pi)^n}\,\frac{1}{k^2}\,\bar{\psi}_v(\vec{p}_2)\gamma_\mu \frac{1}{\not{p}_2 - \not{k} - m} V(\vec{q}) \frac{1}{\not{p}_1 - \not{k} - m}\gamma^\mu\psi_v(\vec{p}_1), \tag{9}$$

with

$$V(\vec{q}) = ie\vec{\gamma}\cdot\frac{\vec{\mu}\times\vec{q}}{8\pi^3|\vec{q}|^2}. \tag{10}$$

Here $\vec{q} = \vec{p_2} - \vec{p_1}$ and the energy component of both four vectors p_1 and p_2 is the valence electron energy ϵ_v. The d^nk integration is easily carried out after Feynman parameterization, using $\alpha_1 = \rho x$ for the electron propagator involving p_1, $\alpha_2 = \rho(1-x)$ for the electron propagator involving p_2, and $\alpha_3 = 1-\rho$ for the photon propagator. This parameterization leads to two combinations of $\vec{p}_1$ and $\vec{p}_2$, $\vec{Q}_1 \equiv (1-\alpha_1)\vec{p}_1 - \alpha_2\vec{p}_2$ and $\vec{Q}_2 \equiv (1-\alpha_2)\vec{p}_2 - \alpha_1\vec{p}_1$. Carrying out the d^nk integration then gives

$$\begin{aligned}\nu_{\rm SE}(A) \;=\; & -\frac{\alpha}{2\pi}\int_0^1 \rho d\rho \int_0^1 dx \int d^3p_2\, d^3p_1\, \bar{\psi}_v(\vec{p}_2)V(\vec{q})\psi(\vec{p}_1)\ln\frac{\Delta_v}{m^2} \\ & -\frac{\alpha}{4\pi}\int_0^1 \rho d\rho \int_0^1 dx \int d^3p_2\, d^3p_1\, \frac{\bar{\psi}_v(\vec{p}_2)N_v\psi(\vec{p}_1)}{\Delta_v},\end{aligned} \tag{11}$$

where

$$\Delta_v = \rho^2\epsilon_v^2 + \rho(m^2-\epsilon_v^2) + \alpha_1\vec{p}_1^{\,2} + \alpha_2\vec{p}_2^{\,2} - |\alpha_1\vec{p}_1 + \alpha_2\vec{p}_2|^2, \tag{12}$$

$$N_v = \gamma_\mu[\not{p}_2(1-\alpha_2) - \alpha_1\not{p}_1 + m]\,V(\vec{q})\,[(1-\alpha_1)\not{p}_1 - \alpha_2\not{p}_2 + m]\gamma^\mu, \tag{13}$$

and an ultraviolet divergent term that cancels with another part of the calculation has been suppressed. As in our previous work we work with stretched states along the quantization z-axis, which allows us to replace $\vec{\mu}$ with $\mu\hat{z}$. The numerators in $\nu_{\rm SE}(A)$ can then be expressed in terms of a number of operators sandwiched between spherical spinors $\chi_{\kappa\mu}(\hat{p})$. They are

denoted as T_A through T_J and are given by

$$\begin{aligned}
T_A &= \chi^\dagger_{\kappa\mu}(\hat{p_2})\vec{\sigma}\cdot(\hat{z}\times\vec{q})\chi_{-\kappa\mu}(\hat{p_1}) \\
T_B &= \chi^\dagger_{-\kappa\mu}(\hat{p_2})\vec{\sigma}\cdot(\hat{z}\times\vec{q})\chi_{\kappa\mu}(\hat{p_1}) \\
T_C &= \chi^\dagger_{\kappa\mu}(\hat{p_2})\vec{\sigma}\cdot(\hat{z}\times\vec{q})\vec{\sigma}\cdot\vec{Q}_2\chi_{\kappa\mu}(\hat{p_1}) \\
T_D &= \chi^\dagger_{-\kappa\mu}(\hat{p_2})\vec{\sigma}\cdot(\hat{z}\times\vec{q})\vec{\sigma}\cdot\vec{Q}_2\chi_{-\kappa\mu}(\hat{p_1}) \\
T_E &= \chi^\dagger_{\kappa\mu}(\hat{p_2})\vec{\sigma}\cdot\vec{Q}_1\vec{\sigma}\cdot(\hat{z}\times\vec{q})\chi_{\kappa\mu}(\hat{p_1}) \\
T_F &= \chi^\dagger_{-\kappa\mu}(\hat{p_2})\vec{\sigma}\cdot\vec{Q}_1\vec{\sigma}\cdot(\hat{z}\times\vec{q})\chi_{-\kappa\mu}(\hat{p_1}) \\
T_G &= \chi^\dagger_{\kappa\mu}(\hat{p_2})\vec{\sigma}\cdot\vec{Q}_1\vec{\sigma}\cdot(\hat{z}\times\vec{q})\vec{\sigma}\cdot\vec{Q}_2\chi_{-\kappa\mu}(\hat{p_1}) \\
T_H &= \chi^\dagger_{-\kappa\mu}(\hat{p_2})\vec{\sigma}\cdot\vec{Q}_1\vec{\sigma}\cdot(\hat{z}\times\vec{q})\vec{\sigma}\cdot\vec{Q}_2\chi_{\kappa\mu}(\hat{p_1}) \\
T_I &= (\hat{z}\times\vec{q})\cdot(\vec{Q}_1+\vec{Q}_2)\chi^\dagger_{\kappa\mu}(\hat{p_2})\chi_{\kappa\mu}(\hat{p_1}) \\
T_J &= (\hat{z}\times\vec{q})\cdot(\vec{Q}_1+\vec{Q}_2)\chi^\dagger_{-\kappa\mu}(\hat{p_2})\chi_{-\kappa\mu}(\hat{p_1})\,. \qquad (14)
\end{aligned}$$

Defining the momentum space wavefunction as

$$\psi_{v\mu}(\vec{p}) = \frac{1}{p}\begin{pmatrix} g_v(p)\chi_{\kappa\mu}(\hat{p}) \\ f_v(p)\chi_{-\kappa\mu}(\hat{p}) \end{pmatrix} \qquad (15)$$

with $v=(n,\kappa)$, the specific equations are, using the abbreviation $g_v(p_i)=g_i$ and $f_v(p_i)=f_i$,

$$\bar{\psi}_v(\vec{p_2})V(\vec{q})\psi(\vec{p_1}) = \frac{1}{p_2p_1}(g_2f_1T_A + f_2g_1T_B) \qquad (16)$$

and

$$\begin{aligned}
N_v = \frac{1}{p_2p_1}\{&(g_2f_1T_A+f_2g_1T_B)[-2m^2+2\epsilon_v^2(1-\rho)^2] - 2\epsilon_v(1-\rho)(g_2g_1T_C+f_2f_1T_D) \\
&-2\epsilon_v(1-\rho)(g_2g_1T_E+f_2f_1T_F) + 2(g_2f_1T_G+f_2g_1T_H) + 4m(g_2g_1T_I - f_2f_1T_J)\}. \qquad (17)
\end{aligned}$$

While we have written these operators for a general magnetic quantum number μ, in the stretched state $\mu = j = 3/2$. We reduce them to functions of p_1, p_2, and the angle between the vectors $\theta = \cos^{-1}(\hat{p_1}\cdot\hat{p_2})$ using a method described in Ref. [15], where a rotation allows three of the four angle integrations to be carried out analytically, leaving only the integration over θ to be evaluated numerically. For $p_{3/2}$ states with $\kappa=-2$, this leads to

$$\begin{aligned}
T_A &= -2[p_2(1-3z^2)+2p_1z] \\
T_B &= -2[p_1(1-3z^2)+2p_2z]
\end{aligned}$$

$$
\begin{aligned}
T_C &= p_1 p_2[3(1-\alpha_2) - 2\alpha_1 + z^2(1+6\alpha_1-\alpha_2)] - 4zp_2^2(1-\alpha_2) - 4z\alpha_1 p_1^2 \\
T_D &= zp_1p_2[5(1-\alpha_2) - 4\alpha_1 - 9z^2(1-\alpha_2)] - 2(1-3z^2)[p_2^2(1-\alpha_2) + \alpha_1 p_1^2] \\
T_E &= p_1 p_2[3(1-\alpha_1) - 2\alpha_2 + z^2(1-\alpha_1+6\alpha_2)] - 4z[p_1^2(1-\alpha_1) + \alpha_2 p_2^2] \\
T_F &= zp_1p_2[5(1-\alpha_1) - 4\alpha_2 - 9z^2(1-\alpha_1)] - 2(1-3z^2)[p_1^2(1-\alpha_1) + \alpha_2 p_2^2] \\
T_G &= -2\alpha_2 p_2^3(1-\alpha_2)(1-3z^2) - 4z\alpha_1(1-\alpha_1)p_1^3 \\
&\quad + p_1^2 p_2[3\alpha_2 - 3\alpha_1^2 + 6\alpha_1 - 3 - 5\alpha_1\alpha_2 + z^2(-6\alpha_1 - 7\alpha_2 - \alpha_1^2 + 7 + 13\alpha_1\alpha_2)] \\
&\quad + zp_1p_2^2[-5\alpha_2^2 + 6\alpha_2 + \alpha_1 - 1 - 5\alpha_1\alpha_2 + z^2(-6\alpha_2 + 3\alpha_1 + 9\alpha_2^2 - 3 - 3\alpha_1\alpha_2)] \qquad (18) \\
T_H &= -2\alpha_1 p_1^3(1-\alpha_1)(1-3z^2) - 4z\alpha_2(1-\alpha_2)p_2^3 \\
&\quad + zp_1^2p_2[6\alpha_1 - 5\alpha_1^2 + \alpha_2 - 5\alpha_1\alpha_2 - 1 + z^2(-6\alpha_1 + 9\alpha_1^2 + 3\alpha_2 - 3\alpha_1\alpha_2 - 3)] \\
&\quad - p_1p_2^2[3(1-\alpha_1) + 5\alpha_1\alpha_2 - 6\alpha_2 + 3\alpha_2^2 + z^2(6\alpha_2 + 7\alpha_1 + \alpha_2^2 - 7 - 13\alpha_1\alpha_2)] \qquad (19) \\
T_I &= 5p_1p_2(1-\rho)(1-z^2) \\
T_J &= 9zp_1p_2(1-\rho)(1-z^2), \qquad (20)
\end{aligned}
$$

where a common factor of $\frac{i}{5}\frac{1}{4\pi}$ is understood.

After this reduction a five dimensional integral remains to be evaluated numerically. We were able to achieve high precision with the program CUHRE, part of the CUBA multidimensional integration package [16]. All other parts of the calculation were carried out in the same manner as our hfs work on the s [9, 17–19] and $p_{1/2}$ states [6]. For brevity, we compress the notation of Ref. [18] as follows. In that work another momentum space integration term called $\nu_{\rm SE}(C)$ was associated with the side diagrams (Figs. 1a and its mirror image): here we combine $\nu_{\rm SE}(A)$ and $\nu_{\rm SE}(C)$ into $\nu_{\rm SE}(p)$, with p standing for momentum space. In [18], another set of terms called $\nu_{\rm SE}(B)$, $\nu_{\rm SE}(D)$, and $\nu_{\rm SE}(E)$ were associated with the subtracted parts of the vertex and side diagrams and were evaluated in coordinate space with partial wave expansions: here we present only the sum as $\nu_{\rm SE}(x)$. The perturbed orbital terms $\nu_{\rm SE}(PO)$ from the side diagrams are unchanged. For the case of vacuum polarization we condense the notation of Ref. [18], where the effect was split into a term coming from perturbed orbitals $\nu_{\rm VP}(PO)$ and a vertex correction $\nu_{\rm VP}(V)$, into their sum. In all cases we follow the convention of presenting the hfs results in units of $(\alpha/\pi)E_F$, where E_F is the lowest-order hyperfine energy. We now turn to the evaluation of QED corrections to hyperfine splitting for the three cases described in the introduction.

III. HYDROGEN ISOELECTRONIC SEQUENCE

One reason for using methods that include all orders in $Z\alpha$ when treating the hydrogen isoelectronic sequence is to carry out comparisons with known $Z\alpha$ expansions. For the $1s$ ground state hfs we were able in Ref. [17] to check our results against the known terms in that expansion, and to evaluate the higher-order $Z\alpha$ terms, a result used in the theory of ground state muonium hfs. In the present case, we would like to determine the coefficients A and B in the formula

$$\nu_{2p_{3/2}} = -\frac{1}{8} + (Z\alpha)^2(A \ln Z\alpha + B) + \ldots, \tag{21}$$

where ν is in unit of $(\alpha/\pi)E_F$ as mentioned in the previous section. The fact that the nonrelativistic wave function vanishes at the origin has eliminated terms present for s states, specifically a term linear in $Z\alpha$ and a squared logarithmic term in the next order.

Even for the ground state problem, high numerical accuracy was required to do the required fitting, as there are severe cancelations between contributing terms and any numerical errors in the data rapidly lead to larger errors in the fitted coefficients. Compounding the problem here is the fact that the coefficients A and B have not to our knowledge been evaluated for the $2p_{3/2}$ state. Our best fits were consistent with a vanishing logarithmic term $A \approx 0$ and a constant term $B \approx -0.5$. Because of numerical problems, the uncertainty in B is high at about 50%, and we cannot rule out a nonvanishing value for A. The cause of these problems is the slow convergence of the partial wave expansion in both the perturbed orbital main term and the subtracted vertex term at low Z. While at higher Z a clear $1/l^3$ behavior was obtained at relatively low l, for low Z the behavior was closer to $1/l^2$ at the highest l's presently obtainable, about $l = 60$. This leads to an uncertainty of about 0.0003 $(\alpha/\pi)E_F$. We note that we were able to eliminate another source of error that had been present in our previous calculations. Specifically, pole terms arising from the vertex graph in which one electron propagator collapsed to a single pole term, but the other remained unaffected, were treated with finite basis set techniques in our previous treatment of s and $p_{1/2}$ hfs. We were able to use differential equation techniques here to eliminate the use of finite basis sets, which converge slowly for this diagram, and the error associated with these pole terms is now negligible. However, it is clear that a more accurate numerical approach is called for, and in the conclusion we will describe possible solutions to this problem.

At higher Z the deviation from $-1/8$ is more pronounced, and our methods are able, as with the s and $p_{1/2}$ cases, to show a strong deviation from the lowest-order value at high Z. In the previous cases a sign change was present, but in this case we start out with a negative contribution that stays negative. We plot the behavior of $\nu_{2p_{3/2}}(SE)$ in Fig. 3 and present a tabulation in Table I, which also includes vacuum polarization results that are not plotted.

IV. NEUTRAL ALKALIS

Turning now to the alkali metal atoms, we first note that some sort of screened potential has to be used. In order to apply S-matrix techniques it has to be a local potential, which rules out the Dirac-Fock potential. We have found that the Kohn-Sham potential, which is local, gives results close to the Dirac-Fock potential. It is defined by

$$U(r) \;=\; -\frac{Z_{eff}(r)\alpha}{r} \;=\; -\frac{Z_{nuc}(r)\alpha}{r} \;+\; \tilde{U}(r), \tag{22}$$

where

$$Z_{eff}(r) \;=\; Z_{nuc}(r) - r\int dr'\,\frac{1}{r_>}\,\rho_t(r') + \frac{2}{3}\left[\frac{81r\rho_t(r)}{32\pi^2}\right]^{1/3} \tag{23}$$

with ρ_t the total charge density for the ground state. At large r, when $Z_{eff}(r)$ is reduced to unity, we freeze it at that value, a procedure known as the Latter correction [20]. The same numerical problems mentioned above carry over to the neutral alkalis, but are of less importance, as we are interested only in the general size of the radiative corrections which, with the important exception of lithium, are much smaller than errors in hfs correlation calculations due to the difficulty of the many-body problem. We summarize our results in Table II. In addition to giving QED corrections coming from closed loop diagrams, we include an effect called $\Delta E_{1\gamma}$, which is the leading non-radiative correction from the difference of the calculation of the structure diagrams of Fig. 2a, which involve the exchange of one photon, with that found in many-body perturbation theory (MBPT) calculations. Here we define MBPT calculations to correspond to an instantaneous Coulomb photon being exchanged, along with intermediate electron propagators restricted to sums over positive energy states, which also affects the counter potential term of Fig. 2b. Because this term can be seen to enter at same same order as the radiative corrections, we have carried out a calculation in which MBPT was redefined to include the instantaneous Breit interaction, but $\Delta E_{1\gamma}$ remained large, indicating that other intrinsically QED corrections play an important

role: we are presently investigating the origin of these corrections. Further discussion of $\Delta E_{1\gamma}$ will be given in the conclusion, but we now focus our attention to the one-loop QED correction, the sum of ν_{SE} and ν_{VP}.

As expected, this correction for neutral lithium is quite close to the $-\frac{\alpha}{8\pi}$ limit, but even though the atoms are neutral, as the nuclear charge increases the feature observed in the hydrogenic case of a rapid increase in magnitude of the effect is present. A notable feature here is the very small contribution of vacuum polarization, which was not negligible in our previous calculations of the s [18] and $p_{1/2}$ [6] states, and can be attributed to the non-penetrating nature of the $p_{3/2}$ states.

Turning to experiment, we first note that a useful complilation of results for alkali $p_{3/2}$ states has recently been given by Das and Natarajan [21]. They do not list any results for lithium, but quote results for sodium, potassium, and rubidium accurate to 162 ppm, 3784 ppm, and 44 ppm respectively. Our radiative corrections for these atoms are 265 ppm, 320 ppm, and 571 ppm, so that the effect is just barely detectable in sodium, beyond detection in potassium, and clearly visible in rubidium, assuming that other sources of theoretical error, most notably those from many-electron correlation effects, can be controlled.

While we will discuss the value for cesium given in Ref. [21] below, we first present another result from Ref. [22],

$$A_{6p_{3/2}} = 50.288\ 27(23)\ \text{MHz}.$$

The accuracy of this experiement, 4.6 ppm, is more than two orders of magnitude smaller than the 1366 ppm QED effect found here for that atom, so although the atom has more electrons than rubidium, the ratio of QED to experimental error is more than ten times larger. Reduction of wave function uncertainties to this level of QED presents a challenge to many-body methods for this atom, which is of considerable interest because of its role in parity nonconservation studies [23]. The Bohr-Weisskopf effect for the $6s$ state is 0.7 percent, for the $6p_{1/2}$ state 803 ppm [6], but for the $6p_{3/2}$ state it is essentially zero, being only about 30 ppb. Thus the hfs of the $6p_{3/2}$ state is an ideal testing ground for relativistic many-body methods, as any complete calculation that leaves out radiative corrections should be larger than experiment by 0.137 percent according to the present calculation. We note that there is a significant experimental discrepancy of 132 ppm between the result we have quoted from

Ref. [22] and that given in Ref. [21],

$$A_{6p_{3/2}} = 50.281\ 63(86)\ \text{MHz},$$

with the latter more than 7 standard deviations away from the former. While a third high accuracy experiment would clearly be useful in resolving this situation, the discrepancy is still more than 10 times smaller than the QED correction calculated here.

Francium is also of interest because of the size of the QED corrections. Instead of the usual tenth of a percent level characteristic of the Schwinger correction, here we see a 0.55 percent correction. While it is very challenging to push any many-body method to the tenth of a percent level, francium has a relatively tractable electronic structure, and if this level of accuracy is reached, the QED correction would be clearly visible. We note that the corrections are even larger for the $7s$ state of francium [18], but in that case one would more likely learn about the nuclear physics of the francium nucleus instead of QED, as the Bohr-Weisskopf effect is large and the nuclear structure relatively poorly known. However, the $7p_{3/2}$ hfs is again almost entirely free of this uncertainty, and, even more so than the $6p_{3/2}$ hfs in cesium, is a promising place to establish the large, nonperturbative change to the Schwinger correction calculated in this paper. The $A_{7p_{3/2}}$ coefficients for ^{212}Fr, ^{221}Fr, and ^{210}Fr have been determined to be 97.2(1) MHz, 65.5(6) MHz, and 78.0(2) MHz respectively [24].

V. LITHIUMLIKE BISMUTH

While a very precise measurement of the ground state hfs of hydrogenic bismuth has been available for quite some time [25],

$$\delta\nu = 5.0840(8)\ \text{eV},$$

and the radiative correction is known to be -0.0413 eV [8], the QED effect is unfortunately difficult to unambiguously extract because of uncertainties in the Bohr-Weisskopf effect, the size of which is somewhat larger than QED. One way of addressing this problem is to study ions in which the nucleus is in a different electronic environment, specifically the three-electron system of lithiumlike bismuth, and make combinations of hfs in the two systems to cancel out the Bohr-Weisskopf uncertainty. As mentioned above, this approach has been

used by Shabaev *et al.* [11], but the experimental situation is inconclusive so far [12]. The present paper suggests a second way to avoid nuclear uncertainty, which is to measure the hfs of the $p_{3/2}$ state of either hydrogenlike or lithiumlike bismuth. In the former case, we predict a fractional shift of -1.978 α/π by interpolating data from Table I, and in the latter -1.800 α/π from a direct calculation. For lithiumlike bismuth, the $A_{2p_{3/2}}$ factor is also corrected by one-photon exchange, a -19.485 α/π fractional correction which changes the lowest-order value of 4.8255 meV to the first-order screened value of 4.6071 meV. If experimental accuracy of well under 0.4 percent can be reached in either case, the large change of the QED correction from the low-Z value should be clearly visible. At present we are not aware of relevant measurements of either ion.

VI. DISCUSSION

In this paper a number of systems involving the hyperfine splitting of $p_{3/2}$ states have been treated. In all cases we stress that because the upper component wave functions of such states has $l = 1$ and the lower $l = 2$, the electron has very little overlap with the nucleus, so that nuclear uncertainties are essentially eliminated.

For the hydrogen isoelectronic sequence a common application of the kind of calculation presented here, which compares all-order $Z\alpha$ binding correction results with the known $Z\alpha$ expansion at low Z, proved difficult. We were able to show that at low Z the expected $-\alpha/8\pi$ correction was present, and the next order terms are $(\alpha/\pi)(Z\alpha)^2(-0.25 + \ldots)$ with no sign of any $\ln Z\alpha$ term present, but numerical noise led to large uncertainties in the fitted results. To attain the needed higher accuracy we are studying the feasiblity of carrying out another subtraction on the vertex diagram, Fig. 1b. Specifically, Eq. (7) would be written as

$$\begin{aligned} S_F V S_F &= S_0 V S_0 + S_0 V S_0 U S_0 + S_0 U S_0 V S_0 \\ &\quad + [S_F V S_F - S_0 V S_0 - S_0 V S_0 U S_0 - S_0 U S_0 V S_0] \end{aligned} \tag{24}$$

where coordinate dependence has been suppressed for brevity. Here V is the hyperfine interaction Hamiltonian and $U = -Z_{nuc}/r + \tilde{U}$ is the effective potential. Beier *et al.* [26] have successfully applied this procedure to the related problem of Zeeman splitting. The basic idea is that the significant contribution of high l terms in the partial wave expansion is due to

short distance near-singularities (the actual ultraviolet divergences having been subtracted out). By doing the above subtraction these short distance near-singularities should be removed. The subtracted term would then be expected to have much faster convergence in terms of the partial wave expansion, and much more accurate results for the part of the calculation carried out in coordinate space would be possible. The extra subtraction terms involving S_0 would have to be carried out with equal accuracy in momentum space, which could be challenging, as this involves evaluating an 8 dimensional integral.

Because of the simplicity of the point-Coulomb problem, an alternative approach that exploits the known analytic expansion of the Dirac-Coulomb propagator in terms of Whittaker functions, very recently applied to calculations of hfs and g-factors in s states [27], is most likely to allow the accurate fits of higher-order $Z\alpha$ terms we have been unable to carry out here. However, for non-point-Coulomb problems the approach described above with extra subtraction terms in Eq. (24) is presumably preferable.

With regard to the neutral alkalis, we consider the results of this paper, which indicate radiative corrections from 0.03 percent for lithium to 0.55 percent for francium, of particular use for tests of many-body perturbation theory (MBPT) techniques. Except for lithium these methods are all that are available for calculations of the alkali metal atoms. Because of the impetus provided by the accurate measurement of parity nonconserving (PNC) transitions in cesium by Wieman *et al.* [23], the question of whether MBPT calculations (which are understood to include different ways of including infinite sets of Brueckner-Goldstone diagrams) can match the experimental accuracy (0.3 percent) is an important one. One way of gauging the accuracy of a method is to compare with standard atomic properties such as ionization energies, transition matrix elements, and hyperfine splitting. However, considerable Bohr-Weisskopf effects enter for both ns and $np_{1/2}$ states, as discussed in Refs. [18, 19] and [6], respectively. Here, on the other hand, no such uncertainty is present, and, in particular, any calculation on cesium that has included the most important diagrams should differ from experiment by 0.137 percent, which corresponds to a change in the hyperfine $A_{6p_{3/2}}$ coefficient of 0.068 MHz.

At this point we elaborate on the role of the $\Delta E_{1\gamma}$ term in Table II. While in principle a full QED calculation of higher-order terms should be carried out, in practice, in order to get high accuracy theoretical predictions for the neutral alkalis, MBPT techniques that include infinite sets of Brueckner-Goldstone diagrams are needed. The relation between these

diagrams and Feynman diagrams gives rise to small corrections that have to be evaluated before a consistent QED treatment can be said to have been given of hfs, or for that matter, any atomic property. While our calculations have been carried out in Feynman gauge, because of the use of a local potential, our results are gauge independent and we could just as well have worked in Coulomb gauge. In Coulomb gauge, two kinds of photon exchange occur, instantaneous Coulomb exchange and transverse photon exchange. While the former corresponds exactly to MBPT, the latter is generally approximated in MBPT as the instantaneous Breit operator. There is in addition an approximation that is also made in MBPT even for Coulomb exchange. When two interactions take place on the same electron line, e.g., a hyperfine interaction and a virtual photon exchange as in Fig. 2a, a full electron propagator, including both positive- and negative-energy intermediate states, is present. However, the negative energy states are generally neglected in MBPT in the *no-pair* approximation. In fact, when considering the way second-order MBPT expressions arise from QED, neglecting negative energy states is in fact essential, as otherwise the summations would involve vanishing denominators, the so-called "Brown-Ravenhall disease" [28], later termed "continuum dissolution" by Sucher [29]. A discussion of these negative energy state contributions, along with references to earlier works, can be found in Ref. [30].

Since QED provides a way to consistently treat negative energy states and the non-instantaneous nature of transverse photon exchange, a possible approach to practical calculations of the neutral alkalis including QED is as follows. We must first suppose that an MBPT method that includes all important Brueckner-Goldstone diagrams has been found. The approximations made to get an MBPT result from QED could then be systematically undone. We have carried out the first step in this paper with our evaluation of $\Delta E_{1\gamma}$, which includes negative energy states and the full transverse photon exchange. The next step would be to treat all two-photon exchange diagrams, an example of which is shown in Fig. 4, using the S-matrix approach of this paper. By isolating those terms with all photons being Coulomb photons and negative energy states removed, the difference in these two-photon exchange diagrams would be identified as $\Delta E_{2\gamma}$. If this contribution turned out to be small, and reasonable arguments could be found to justify the assumption that the analogous contributions $\Delta E_{n\gamma}$ with $n \geq 3$ were also small, MBPT and QED could be joined together. However, considerable theoretical work, both in MBPT and in QED, remains to be done before this program could be implemented. We note here an alternative approach

developed by Lindgren and collaborators [31], which also addresses the issue of combining QED and the many-body problem.

We turn finally to lithiumlike and hydrogenic bismuth, where the $1/Z$ expansion allows one to work with a pure QED approach, as two-photon diagrams will be suppressed by a factor $1/Z$. A great deal of experimental and theoretical effort has gone into the study of these ions, but to date the large QED change from the Schwinger correction has not been established because of nuclear physics uncertainties. We feel that the freedom from these uncertainties provided by the study of $p_{3/2}$ states warrants serious experimental effort to measure hyperfine splitting for such states.

Acknowledgments

The work of J.S. was supported in part by NSF Grants No. PHY-0451842 and PHY-0757125. The work of K.T.C. was performed under the auspices of the U.S. Department of Energy by Lawrence Livermore National Laboratory under Contract DE-AC52-07NA27344.

---

[1] B. Odom, D. Hanneke, B. D'Urso, and G. Gabrielse, Phys. Rev. Lett. **97**, 030801 (2006).

[2] H.M. Foley and P. Kusch, Phys. Rev. **73**, 412 (1948).

[3] J.E. Nafe, E.B. Nelson, and I.I. Rabi, Phys. Rev. **71**, 914 (1947).

[4] J. Schwinger, Phys. Rev. **73**, 416 (1948).

[5] S.J. Brodsky and R.G. Parsons, Phys. Rev. **176**, 423 (1965).

[6] J. Sapirstein and K.T. Cheng, Phys. Rev. A **74**, 042513 (2006).

[7] A. Bohr and V.F. Weisskopf, Phys. Rev. **77**, 94 (1950).

[8] H. Persson, S.M. Schneider, W. Greiner, G. Soff, and I. Lindgren, Phys. Rev. Lett. **76**, 1433 (1996).

[9] S.A. Blundell, K.T. Cheng, and J. Sapirstein, Phys. Rev. A **55**, 1857 (1997).

[10] V.M. Shabaev, M. Tomaselli, T. Kuhl, A.N. Artemyev, and V.A. Yerokhin, Phys. Rev. A **56**, 252 (1997).

[11] V. Shabaev, A.N. Artemyev, V.A. Yerokhin, O.M. Zherebtsov, and G. Soff, Phys. Rev. Lett. **86**, 3959 (2001).

[12] P. Beiersdorfer, G.V. Brown, H. Chen, M.H. Chen, K.T. Cheng, J. Clementson, P.T. Springer, D.B. Thorn, E. Träbert, and J. Sapirstein (unpublished).

[13] W.H. Furry, Phys. Rev. **81**, 115 (1951).

[14] J. Sapirstein, Rev. Mod. Phys. **70**, 55 (1998).

[15] Lars Hambro, Phys. Rev. A **6**, 865 (1972).

[16] T. Hahn, Comput. Phys. Commun. **168**, 78 (2005).

[17] S.A. Blundell, K.T. Cheng, and J. Sapirstein, Phys. Rev. Lett. **78**, 4914 (1997).

[18] J. Sapirstein and K.T. Cheng, Phys. Rev. A **67**, 022512 (2003).

[19] J. Sapirstein and K.T. Cheng, Phys. Rev. A **63**, 032506 (2001).

[20] R. Latter, Phys. Rev. **99**, 510 (1957).

[21] D. Das and V. Natarajan, J. Phys. B **40**, 035001 (2008).

[22] Vladisov Gerginov, Andrei Derivianko, and Carol E. Tanner, Phys. Rev. Lett. **91**, 072501 (2003).

[23] S.C. Bennett and C.E. Wieman, Phys. Rev. Lett. **82**, 2484 (1999); C.S. Wood, S.C. Bennett, D. Cho, B.P. Masterson, J.L. Roberts, C.E. Tanner, and C.E. Wieman, Science **275**, 1759 (1997).

[24] J.E. Sansonetti, J. Phys. Chem. Ref. Data **36**, 497 (2007).

[25] I. Klaft, S. Borneis, T. Engel, B. Fricke, R. Greiser, G. Huber, T. Kuhl, D. Marx, R. Neumann, S. Schroder, P. Seelig, and L. Volker, Phys. Rev. Lett. **73**, 2425 (1994).

[26] T. Beier, I. Lindgren, H. Persson, S. Salomonson, P. Sunnergren, H. Häffner, and N. Hermanspahn, Phys. Rev. A **62**, 032510 (2000).

[27] V.A. Yerokhin and U.D. Jentschura, Phys. Rev. Lett. **100**, 163001 (2008).

[28] G. E. Brown and D. G. Ravenhall, Proc. R. Soc. London, Ser. A **208**, 552 (1951).

[29] J. Sucher, Phys. Rev. A **22**, 348 (1980).

[30] J. Sapirstein, K. T. Cheng, and M. H. Chen, Phys. Rev. A **59**, 259 (2001).

[31] I. Lindgren, S. Salomonson, and D. Hedendahl, Phys. Rev. A **73**, 062502 (2006).

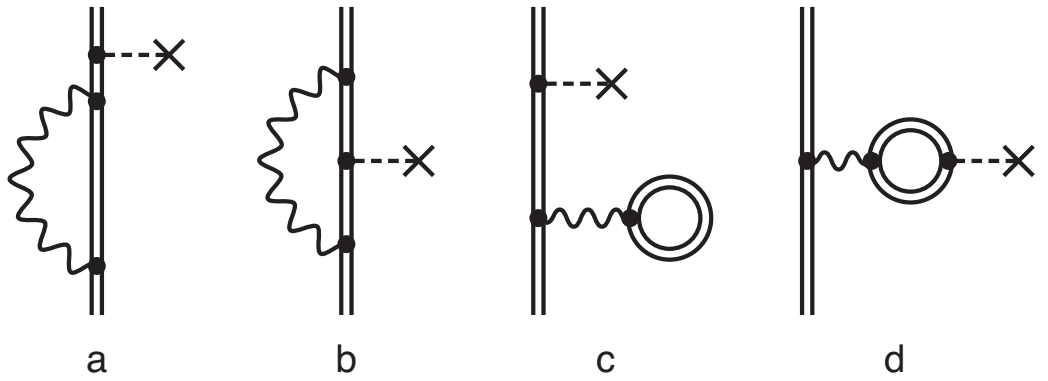

FIG. 1: One-loop self-energy and vacuum polarization diagrams. Dashed lines that end with crosses are hyperfine interactions. Wavy lines are virtual photons.

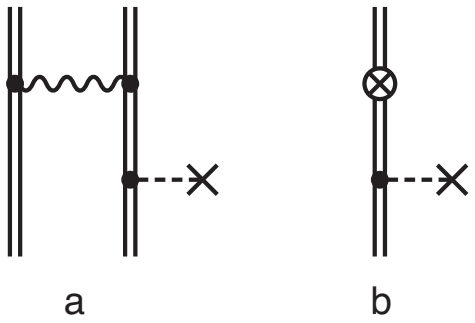

FIG. 2: One-photon exchange correlation diagrams. Dashed lines that end with crosses are hyperfine interactions. The wavy line is a virtual photon. The symbol $\otimes$ represents interaction with the counter potential $\tilde{U}(r)$.

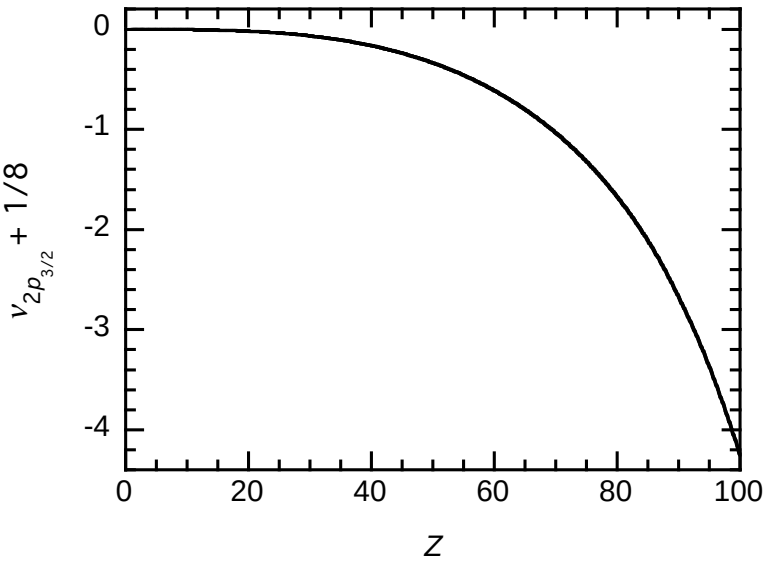

FIG. 3: Self-energy contributions to the $2p_{3/2}$ hfs for hydrogenic ions in units of $(\alpha/\pi)E_F$.

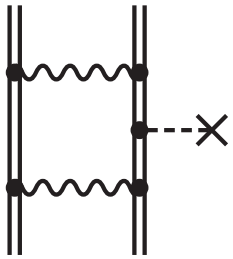

FIG. 4: Typical two-photon exchange correlation diagrams. The dashed line that ends with a cross is hyperfine interaction. Wavy lines are virtual photons.

TABLE I: Breakdown of QED radiative contributions to $2p_{3/2}$ hfs. Units: $(\alpha/\pi)E_F$.

Z	$\nu_{\rm SE}(PO)$	$\nu_{\rm SE}(p)$	$\nu_{\rm SE}(x)$	$\nu_{\rm SE}$	$\nu_{\rm VP}$
1	0.0000	0.7403	-0.8657	-0.1254	0.0000
2	0.0012	0.7376	-0.8636	-0.1249	0.0000
3	0.0016	0.7337	-0.8612	-0.1259	0.0000
4	0.0032	0.7291	-0.8581	-0.1259	0.0000
5	0.0052	0.7238	-0.8544	-0.1255	0.0000
6	0.0068	0.7179	-0.8507	-0.1259	0.0000
7	0.0089	0.7116	-0.8461	-0.1255	0.0000
8	0.0112	0.7046	-0.8416	-0.1257	0.0000
9	0.0137	0.6979	-0.8369	-0.1253	0.0000
10	0.0161	0.6906	-0.8339	-0.1271	0.0000
20	0.0445	0.6085	-0.7951	-0.1421	0.0005
30	0.0739	0.5204	-0.7822	-0.1880	0.0016
40	0.0984	0.4328	-0.8153	-0.2841	0.0038
50	0.1128	0.3483	-0.9147	-0.4537	0.0072
60	0.1121	0.2673	-1.1054	-0.7260	0.0125
70	0.0911	0.1901	-1.4232	-1.1420	0.0200
80	0.0438	0.1163	-1.9263	-1.7662	0.0303
90	-0.0376	0.0457	-2.7207	-2.7126	0.0445
100	-0.1631	-0.0223	-3.9917	-4.1770	0.0618

TABLE II: Vacuum polarization (VP) and self-energy (SE) contributions to hfs for $np_{3/2}$ states of the alkalis. QED is the sum of VP and SE, and $\Delta E_{1\gamma}$ is the difference between the QED diagrams of Fig. 2 and first-order MBPT restricted to instantaneous Coulomb photon exchanges. Units: $(\alpha/\pi)E_F$.

	^{7}Li	^{23}Na	^{39}K	^{87}Rb	^{133}Cs	^{223}Fr
$\nu_{\rm VP}(V)$	0.000	0.000	0.000	0.001	0.004	0.017
$\nu_{\rm VP}(PO)$	0.000	0.000	0.000	0.002	0.006	0.026
$\nu_{\rm VP}$	0.000	0.000	0.000	0.003	0.010	0.043
$\nu_{\rm SE}(PO)$	0.001	0.017	0.049	0.151	0.256	0.433
$\nu_{\rm SE}(p)$	1.109	4.718	6.289	7.688	8.429	9.024
$\nu_{\rm SE}(x)$	−1.238	−4.849	−6.475	−8.084	−9.283	−11.899
$\nu_{\rm SE}$	−0.128	−0.114	−0.138	−0.246	−0.598	−2.442
QED	−0.128	−0.114	−0.138	−0.243	−0.588	−2.399
$\Delta E_{1\gamma}$	−0.014	0.235	0.201	0.455	1.072	4.781